Prodromal local sleep disorders in a rat model of Parkinson's disease cholinopathy, hemiparkinsonism and hemiparkinsonism with cholinopathy

Jelena Petrovic*, Ljiljana Radovanovic, Jasna Saponjic

Institute for Biological Research – Sinisa Stankovic – National Institute of Republic of Serbia, Department of Neurobiology, University of Belgrade, Belgrade, Serbia

*Corresponding Author:

Jelena Petrovic, Ph.D.
Department of Neurobiology,
Institute for Biological Research – Sinisa Stankovic,
National Institute of Republic of Serbia
Despot Stefan Blvd., 142
11060 Belgrade, Serbia.
(Phone) + 381 11 2078426
(Fax) + 381 11 2761433
E-mail: jelena.petrovic@ibiss.bg.ac.rs

Abstract

We investigated the prodromal alterations of local sleep, particularly the motor cortical and hippocampal sleep, along with spontaneous locomotor activity in the rat models of Parkinson's disease (PD).

We performed our experiments in adult, male Wistar rats, chronically implanted for sleep recording and divided into four experimental groups: the control (implanted controls), the bilateral pedunculopontine tegmental nucleus (PPT) lesions (PD cholinopathy), the unilateral substantia nigra pars compacta (SNpc) lesions (hemiparkinsonism) and the unilateral SNpc/bilateral PPT lesions (hemiparkinsonism with PD cholinopathy). We followed their sleep, basal locomotor activity and spatial habituation for 14 days following the surgical procedures.

Severe prodromal local sleep disturbances in the hemiparkinsonian rats were expressed as sleep fragmentation and distinct local NREM/REM EEG microstructure alterations in both the motor cortex and the hippocampus. Alongside the state-unrelated role of the dopaminergic control of theta oscillations and NREM/REM related sigma and beta oscillations, we demonstrated that the REM neurochemical regulatory substrate is particularly important in the dopaminergic control of beta oscillations. In addition, hippocampal prodromal sleep disorders in the hemiparkinsonian rats were expressed as NREM/REM fragmentation and the opposite impact of dopaminergic versus cholinergic control of the NREM delta and beta oscillation amplitudes in the hippocampus, likewise in the motor cortex versus the hippocampus.

All these distinct prodromal local sleep disorders and the dopaminergic vs. cholinergic impact on NREM/REM EEG microstructure alterations are of fundamental importance for the further development and follow-up of PD-modifying therapies, and for the identification of patients who are at risk of developing PD.

Keywords: hemiparkinsonism, local sleep disorder, motor cortex, hippocampus, Parkinson's disease cholinopathy, rat

1. Introduction

Neurodegenerative diseases are a heterogeneous group of age-related disorders characterized by the slow but irreversible deterioration of brain functions due to the selective death of distinct neuronal populations (Błaszczyk, 2016). As the human population is getting older, neurodegenerative diseases, such as Alzheimer's disease (AD) and Parkinson's disease (PD), are becoming more common (GBD 2016 Parkinson's Disease Collaborators, 2018; Mayeux and Stern, 2012).

There is no doubt that during aging all the functional domains undergo a physiological decline, but the precise process of when and how the compensatory mechanisms become insufficient to overcome the aging induced alterations, leading from impaired function of the brain system during normal aging to neurodegeneration, is still poorly understood.

It is well-known that PD is a progressive multisystem neurodegenerative disease characterized by distinct motor and non-motor symptoms, reflecting the localization and progression of the underlying pathology (Blesa and Przedborski, 2014). Motor impairment involves a spectrum of movement and posture abnormalities including bradykinesia, rigidity, resting tremor, posture, and gait problems (Andrzejewski et al., 2016). These symptoms are classically and primarily linked to a progressive loss of the substantia nigra pars compacta (SNpc) dopaminergic (DA) neurons and the consequent striatal DA level reduction (Błaszczyk, 2016; Blesa and Przedborski, 2014). Although motor impairment is one of the main pathological hallmarks of PD, indicating the onset of clinical Parkinsonism, this occurs rather late, following a severe nigrostriatal dopaminergic neurodegeneration (being an approximately 60% loss of the nigral DA neurons and 80% loss of the striatal DA neurons) (Videnovic et al., 2013), which reduces the possibility of any effective medical treatment.

However, PD pathology extends beyond the loss of the dopaminergic pathway. Other brain systems (including the serotonergic, noradrenergic, cholinergic, GABAergic and glutamatergic systems) are also affected and associated with many of the non-motor symptoms, such as impaired olfaction, depression, cognitive changes, dementia and sleep disturbances (Blesa and Przedborski, 2014; Schapira et al., 2017). Many of these non-motor features may precede the onset of motor symptoms by years or even decades, providing a unique opportunity to study the progression of PD, potential prodromal marker identification, presymptomatic screening and possible early therapeutic interventions (Schapira et al., 2017).

Alterations to the pedunculopontine tegmental nucleus (PPT) cholinergic pathways have been related to impaired cognition, frequent falling, gait problems, and sleep disorders in PD (Bohnen and Albin, 2011; Bohnen et al., 2012; Ciric et al., 2016, 2017, 2018; Müller et al.,

2013; Petrovic et al., 2013a, 2013b, 2014). With a prevalence of 60-70%, sleep disturbances are among the most frequent non-motor symptoms in PD patients (Medeiros et al., 2019; Schapira et al., 2017). As demonstrated by various clinical studies, REM sleep behavioral disorder (RBD) is frequently encountered in PD as an early characteristic of the underlying pathology, which preceds the motor symptoms (Boeve et al., 2007; Boucetta et al., 2016; Iranzo et al., 2006; Videnovic et al., 2013). It has been suggested that RBD results from an alteration of the REM sleep regulatory circuits within the brainstem which are involved in the promotion of REM sleep and muscle atonia (Boucetta et al., 2016; Iranzo et al., 2006). Being the high relay nucleus for the overall control of REM sleep phenomenon, including REM atonia (Datta and MacLean, 2007), the PPT is probably involved in RBD genesis and could be severely affected in PD pathology (Perez-Lloret and Barrantes, 2016). Neuropathological studies in humans align with these findings, reporting a degeneration of about 50% of the PPT cholinergic neurons in PD patients (Bohnen and Albin, 2011).

Additional evidence is provided by basic studies, supporting the association between sleep disturbance and PPT cholinergic denervation in PD. In particular, recent studies in the rat model of PD cholinopathy have demonstrated local alterations in NREM/REM EEG oscillations, cortical drives and sleep spindle dynamics as the earliest functional biomarkers of PD, preceding hypokinesia (Ciric et al., 2016, 2017, 2018; Petrovic et al., 2013a, 2013b, 2014) and the emergence of two distinct REM states with functionally differential total EMG power, local EEG microstructure, and the sensorimotor and motor cortical drives to the dorsal nuchal muscles (Petrovic et al., 2014).

Moreover, severe sleep disturbances have also been shown in hemiparkinsonian rats, where the dopaminergic denervation induced by the SNpc lesion was related to long-lasting sleep fragmentation, NREM/REM theta amplitude augmentation and altered NREM/REM-related sleep spindles and high voltage sleep spindle dynamics (Ciric et al., 2019).

Therefore, since both the cholinergic and the dopaminergic systems are compromised in PD pathology and associated with severe sleep disturbance, we aimed this study to investigate the prodromal alterations of local sleep, particularly motor cortical and hippocampal sleep, along with spontaneous locomotor activity in rats following the bilateral PPT lesion (PD cholinopathy), the unilateral SNpc lesion (hemiparkinsonism) and in rats with the combined unilateral SNpc/bilateral PPT lesion (hemiparkinsonism complicated with PD cholinopathy).

2. Material and Methods

2.1. Experimental Design

The experiments were performed on 32 adult male Wistar rats (each two-and-a-half month old, weighing between 250 and 290 g), which were chronically implanted for sleep recording. The rats were randomly divided into four experimental groups: a control group (with implanted controls, n=8), a bilateral PPT lesion group (with rat model of PD cholinopathy, n=8), a unilateral SNpc lesion group (being hemiparkinsonian rats, n=8) and a unilateral SNpc/bilateral PPT lesion group (being hemiparkinsonian rats with PD cholinopathy, n=8). We followed the sleep, basal locomotor activity and spatial habituation (as an indirect measure of memory abilities) of the rats for 14 days following the surgical procedure. All the behavioral assessments were performed a week after the sleep recording session and during the same circadian phase as the sleep recording (during the inactive circadian phase for rats, from 9 a.m. to 3 p.m.). For the behavioral assessments, we included an additional control group of untreated rats of the same age as all the other experimental groups (physiological control, n=6). The experimental time-line is depicted in **Fig. 1**.

After the surgery and throughout the experimental protocol, the animals were individually housed in custom-made clear plexiglass cages (30 × 30 × 30 cm) on a 12 hour light–dark cycle (7 a.m. lights on, 7 p.m. lights off) at 25ºC. Food and water were available *ad libitum*.

All the procedures were performed in accordance with EEC Directive (2010/63/EU) on the Protection of Animals Used for Experimental and other Scientific Purposes, and the protocol was approved by the Ethical Committee for the Use of Laboratory Animals of the Institute for Biological Research “Siniša Stanković” – National Institute of Republic of Serbia, University of Belgrade (Approval No. 2-21/10).

2.2. Surgical Procedure

The surgical procedures employed for the chronic electrode implantation for sleep recording have been described previously (Ciric et al., 2018, 2019; Petrovic et al., 2013a, 2013b, 2014) and are outlined below.

Two-and-a-half month old Wistar rats were anesthetized intraperitoneally with ketamine/diazepam anesthesia (50 mg/kg, Zoletil® 50, VIRBAC, France) and placed in a stereotaxic frame (Stoelting Co., Europe). We implanted two epidural stainless-steel screw electrodes for the recording of cortical EEG activity from the motor cortex (MCx; A/P: +1.0 mm from the bregma; R/L: 2.0 mm from the sagittal suture; D/V: 1.0 mm from the skull), and two stainless-steel teflon-coated wires (Medwire, NY, USA) into the CA1 hippocampal regions (Hipp; A/P: −3.6 mm from the bregma; R/L: 2.5 mm from the sagittal suture; D/V: 2.5 mm from the brain surface, following Paxinos and Watson, 2005) for the recording of hippocampal

EEG activity. Bilateral wire electrodes were implanted into the dorsal nuchal musculature to assess skeletal muscle activity (EMG) and a stainless-steel screw electrode was implanted in the nasal bone as a ground. All the electrode leads were soldered to a miniature connector plug (39F1401, Newark Electronics, Schaumburg, IL, USA) and the assembly was fixed to the screw electrodes and skull using acrylic dental cement (Biocryl-RN, Galenika a.d. Beograd, Serbia).

All the lesions were performed during the same surgical procedure for the implementation of the EEG and EMG electrodes. PD cholinopathy in Wistar rats was induced through a bilateral PPT lesion, whereas hemiparkinsonism was induced through a unilateral SNpc lesion. To induce hemiparkinsonism with PD cholinopathy, we performed double lesioning, in this case both a unilateral SNpc lesion and a bilateral PPT lesion. Sterotaxically guided microinfusions of ibotenic acid, used for the PPT lesions (IBO, Sigma-Aldrich, St. Louis, MO, USA), or 6-hydroxy dopamine hydrobromide salt, used for the SNpc lesions (6-OHDA, Sigma-Aldrich, St. Louis, MO, USA), were performed using a Digital Lab Standard Stereotaxic Instrument (Stoelting Co., Europe) with a Quintessential Stereotaxic Injector (Stoelting Co., Wood Dale, IL, USA) and a Hamilton syringe (10 µl). The IBO and 6-OHDA concentrations/volumes were chosen on the basis of previous studies (Ciric et al., 2016, 2019; Gilmour et al., 2011; Inglis and Semba, 1997; Oliveira et al., 2017; Petrovic et al., 2013a, 2013b, 2014; Pienaar and van de Berg, 2013; Rodriguez et al., 1999). The bilateral PPT lesion was performed using 0.1 M IBO/0.1 M of phosphate buffered saline (PBS), infused bilaterally into the PPT (A/P: −7.8 mm from the bregma; R/L: 1.9 mm from the sagittal suture; D/V: 7.0 mm from the brain surface, following Paxinos and Watson, 2005). The IBO microinfusions were introduced at a volume of 100 nl, as a continuous infusion over 60 seconds. The unilateral SNpc lesion was performed using 2 µl of 6 µg/µl 6-OHDA, dissolved in ice cold sterile saline (0.9% NaCl), and supplemented with 0.2% ascorbic acid, which served as an anti-oxidant, into the right SNpc (A/P: −5.3 mm from the bregma; R: 2.4 mm from the sagittal suture; D/V: 7.4 mm from the brain surface, following Paxinos and Watson, 2005). The 6-OHDA microinfusions were performed as a continuous infusion of 200 nl/min at a constant flow rate, over 10 minutes (Ciric et al., 2019; Rajkovic et al., 2019). In order to minimize the uptake of 6-OHDA by the noradrenergic neurons, 30 minutes prior to the microinfusion, each rat received a bolus of desipramine hydrochloride (28.42 mg/kg, i.p., Sigma-Aldrich, Germany; pH = 7.4). Following each microinfusion the needle was left within the local brain tissue for 5 minutes before its removal from the brain, allowing the solution to diffuse within the PPT or SNpc. For the bilateral PPT lesions, the Hamilton syringe needle was always washed out following the first

IBO microinfusion into the PPT, and before the microinfusion into the PPT of the other brain side.

2.3. Recording Procedure

At the end of the surgical procedure, the scalp wounds were sutured and the rats were allowed to recover for 13 days before their adaptation to the recording cable for one day. The sleep recording sessions of spontaneous sleep were performed in all rats 14 days after the surgical procedure.

Sleep recordings were performed for 6 hours during the light phase, starting at 9 a.m. The EEG and EMG activities were carried from the connector plug on the rat head by a cable, passed through a sealed port on the recording box, and differentially recorded. The differential mode consisted of 6 inputs (left MCx, right MCx, left Hipp, right Hipp, left EMG and right EMG), each with a (+) on the left and a (−) on the right side, and all with the same ground (a screw electrode implanted in the nasal bone) (Ciric et al., 2015, 2016, 2018, 2019; Saponjic et al., 2016). After conventional amplification and filtering (0.3–100 Hz band pass; A-M System Inc. Model 3600, Carlborg, WA, USA), the analogue data was digitized (at a sampling frequency of 256/s) using DataWave SciWorks Experimenter Version 8.0 (DataWave Technologies, Longmont, CO, USA), and the EEG and EMG activities were displayed on a computer monitor and stored on a disk for further off-line analysis (Ciric et al., 2015, 2016, 2018, 2019; Petrovic et al., 2013a, 2013b, 2014; Saponjic et al., 2016).

2.4. Behavioral Assessments

Behavioral assessments were carried out a week after the sleep recording session, during the same circadian phase as for the previous sleep recording session (from 9 a.m. to 3 p.m.). The behavioral tests included basal locomotor activity, stereotypic activity, vertical activity and spatial habituation. Before each test, the animals were allowed to habituate for 30 minutes to the experimental room (which had quiet, homogenous lighting). For each animal, the locomotor, stereotype-like and vertical activities were examined over 30 minutes , using Opto-Varimex Auto-Track System in a 43 x 43 cm square arena (Columbus Instruments, OH, USA) (Ciric et al., 2018, 2019). The spatial habituation test was performed over three consecutive days (30 minutes in the open arena each day), separated by 24 hour intervals, and served as an indirect measure of the spatial memory abilities of the rats (Ciric et al., 2019).

We should note here that for all the behavioral assessments we included an additional group of untreated rats (**Fig. 1;** non-implanted, non-lesioned rats; the physiological control group; n=6).

2.5. Tissue Processing and Immunohistochemistry

At the end of all the recording and behavioral assessments, the lesions were verified and quantified. All the rats were deeply anesthetized and perfused transcardially, starting with a vascular rinse until the liver had been cleared (using 200 ml of 0.9% saline at a perfusion speed of 40 ml/min); followed by a 4% paraformaldehyde solution (PFA) in 0.1 M PBS (200 ml; initially 100 ml at 40 ml/min, and then 30 ml/min), and finally with a 10% sucrose solution in 0.1 M PBS (200 ml at 30 ml/min). The animals were sacrificed and the brains were extracted, cleared of the meninges and blood vessels, and immersed in 4% PFA overnight, and then in a 30% sucrose solution for several days. The brains were cut in the coronal plane into 40 μm-thick sections using a cryotome (Leica, Wetzlar, Germany), and the free-floating sections were further stored in a cryoprotective buffer (0.05 M phosphate buffered, 25% glycerol, and 25% ethylene glycol) at -20°C (Ciric et al., 2017, 2018, 2019).

The PPT lesion was identified using NADPH – diaphorase histochemistry and quantified based on the number of NADPH – diaphorase positively stained cells within the PPT (Paxinos et al., 2009). Briefly, the free-floating sections were rinsed in 0.1 M PBS, pH = 7.4, and incubated for 1 hour at 37°C in the staining solution – a mixture of the substrate solution with β-nicotinamide adenine dinucleotide phosphate, reduced Na4 salt (β-NADPH, Serva, Heidelberg, Germany), and dimethyl sulfoxide (DMSO, Sigma-Aldrich, Germany). The substrate solution contained dissolved nitro blue tetrazolium chloride (NBT, Serva, Heidelberg, Germany), and 5bromo-4chloro-3indolyl phosphate (BCIP, Serva, Heidelberg, Germany) in the substrate buffer at pH = 9.5 (0.1 M Tris, 100 mM NaCl, 5 mM $MgCl_2$). To reduce the background staining coming from the endogenous alkaline phosphate, the specific inhibitor levamisole (Sigma-Aldrich, Germany) was added to the staining solution to produce the final concentration of 2 mM (Ciric et al., 2016; Lazic et al., 2015; Petrovic et al., 2013a). Finally, all the sections were mounted on slides and placed in a clearing agent (Xylene, Zorka Pharma, RS), coverslipped using DPX (Sigma-Aldrich, USA), and examined under a Zeiss Axiovert microscope with a camera.

The SNpc dopaminergic neuronal loss was identified by TH immunohistochemistry, and quantified based on the number of TH immunostained cells within the SNpc. The brain sections were initially thoroughly rinsed with 0.1 M PBS. The endogenous peroxidase activity was neutralized using 3% hydrogen peroxide/10% methanol in 0.1 M PBS for 15 min, and non-specific binding was prevented by 60 minutes of incubation in 5% normal donkey serum (D9663, Sigma-Aldrich USA)/0.1 M PBS at RT (Ciric et al., 2018). The sections were further incubated for 48 hours at +4°C with a primary mouse monoclonal anti-TH antibody (dil. 1:16000, T2928, Sigma-Aldrich, USA) in a blocking solution with 0.5% Triton X-100, and

subsequently for 90 minutes in polyclonal rabbit anti-mouse immunoglobulin (dil. 1:100, Agilent Dako, P0260, Denmark). Between each immunolabeling step, the sections were washed in fresh 0.1 M PBS (3 x 5 min). The immunoreactive signals were visualized using a diaminobenzidine solution [1% 3,3'–diaminobenzidine (11208, Acros organics, Belgium)/0.3% hydrogen peroxide/0.1 M PBS]. All the sections were finally mounted on slides, dehydrated in a series of increasing ethanol solutions (Ethanol 70%, 96%, 100%, Zorka Pharma, RS), placed in a clearing agent (Xylene, Zorka Pharma, RS), mounted with DPX (Sigma-Aldrich, USA), coverslipped and examined under a Zeiss Axiovert microscope with a camera. To test the specificity of the immunolabeling, the primary antibodies were omitted in the control experiments.

The quantification of cholinergic and/or dopaminergic neuronal loss was conducted using ImageJ 1.46 software by counting the NADPH – diaphorase or TH positively stained cells. For this purpose, all the tissue samples of the corresponding experimental group and brain structure were grouped into three stereotaxic ranges of the overall PPT or SNpc rostro-caudal dimension. The stereotaxic ranges defined for the SNpc lesion were: 4.60–5.10; 5.20–5.70; and 5.80–6.30 mm caudally from the bregma. The stereotaxic ranges defined for the PPT lesion were: 6.90–7.40; 7.50–8.00; and 8.10–8.60 caudally from the bregma. The unilateral SNpc lesions were quantified with respect to its corresponding contralateral SNpc. In particular, for each brain and each defined stereotaxic range, the dopaminergic neuronal loss in the corresponding experimental group was expressed with respect to the mean contralateral control absolute number of TH positive cell, taken as 100% (Ciric et al., 2019). The bilateral PPT lesions were quantified with respect to the controls. To be specific, for each brain and each defined stereotaxic range, the cholinergic neuronal loss in the corresponding experimental group was expressed for each brain side with respect to the corresponding mean absolute number of NADPH – diaphorase positive cells in the controls, taken as 100% (Ciric et al., 2016; Lazic et al., 2015; Petrovic et al., 2013a).

The number of NADPH – diaphorase and TH positively stained cells, counted in this way, was intended to provide an estimation of neuronal loss rather than to determine the absolute number of the cholinergic and dopaminergic neurons.

2.6. Sleep Analysis

The sleep analysis was done using software developed in MATLAB 6.5 (Ciric et al., 2015, 2016; Lazic et al., 2015, 2017; Petrovic et al., 2013a, 2013b, 2014), and upgraded to MATLAB R2011a (Ciric et al., 2017, 2018, 2019).

2.6.1. Differentiation of the sleep/wake states

We applied Fourier analysis to the signals acquired throughout each 6-hour recording (2160 10 seconds Fourier epochs in total) and each 10 second epoch was differentiated, based on the EEG and EMG, as being a Wake, NREM or REM state (Ciric et al., 2015, 2016, 2019; Lazic et al., 2015, 2017; Petrovic et al., 2013a, 2013b, 2014; Saponjic et al., 2016). The differentiation was achieved in two steps. First, by using the motor cortical or hippocampal EEG, we extracted all the 10 second Wake epochs from each 6-hour recording, based on the product of sigma and theta frequency power on the y-axis, and EMG power on the x-axis (Petrovic et al., 2013a, 2013b, 2014). Further, the differentiation of the NREM and REM 10 second epochs was done using the EMG power on the y-axis, and the delta/theta power ratio on the x-axis (Petrovic et al., 2013a, 2013b, 2014). The differentiation of all the Wake/NREM/REM epochs was improved by using the logarithmic values of the quantities on both axes, and was finally achieved using the two clusters K means algorithm (Ciric et al., 2015, 2016; Lazic et al., 2015, 2017; Petrovic et al., 2013a, 2013b, 2014; Saponjic et al., 2016).

To assess the local sleep (notably the local sleep architecture and the local state-related EEG microstructure) we particularly extracted the simultaneous (common) and non-simultaneous (uncommon) Wake/NREM/REM 10 second epochs of the motor cortex and the hippocampus. (Ciric et al., 2018, 2019).

In addition, we also analyzed the motor cortical and hippocampal Wake/NREM/REM episode dynamics. The average "episode" duration of each state was calculated by concatenating all the bouts of each state and by dividing the total duration obtained by the number of all the bouts (10 seconds, 20 seconds, 30 seconds, and so on) and expressed as mean ± SE in minutes. In this, we consider as an episode every single 10 seconds of Wake/NREM/REM (a 10 second "episode") or a number of the consecutive 10 second epochs of the same state (20 second or 30 second "episodes", and so on). Although the classical term "episode" is not entirely appropriate to our form of data analysis (Ciric et al., 2015, 2016, 2019; Lazic et al., 2017) we have retained this term as it is conventional.

2.6.2. Sleep state related EEG analysis

To assess the local sleep/wake state-related EEG amplitude changes (the EEG microstructure), we calculated the group probability density distributions of all the common Wake, NREM and REM relative amplitudes over 6 hours, using the Probability Density Estimate (PDE) routine supplied with MATLAB R2011a (Ciric et al., 2018, 2019). The analysis included conventional EEG frequency bans (δ = 0.3-4 Hz; θ = 4.1-8 Hz; σ = 10.1-15 Hz; β = 15.1-30 Hz; γ = 30.1-50 Hz).

In order to eliminate any influence from absolute signal amplitude variations on the recordings, we computed the relative Fourier amplitudes as follows (Petrovic et al., 2013a, 2013b, 2014):

$$(RA)_b = \frac{\sum_b Amp}{\sum_{tot} Amp}, \quad b=\{\delta, \theta, \sigma, \beta, \gamma\}.$$

In addition, for each sleep/wake state and each frequency band, PDE analysis was performed on the assembles of relative amplitudes (Lazic et al., 2015, 2017; Petrovic et al., 2013a, 2013b) by pooling the measured values from all the animals belonging to the specific experimental group. For statistical analysis of the relative amplitudes/6 hours, we calculated the means during each 30 minutes for Wake and REM, and during each 60 minutes for NREM. Here, we particularly analyzed the PDE/6 hours of common motor cortical and hippocampal NREM and REM sleep.

2.7. Statistical Analysis

All statistical analyses were performed using a Kruskal-Wallis ANOVA (χ^2 values) with the Mann Whitney U (z values) two-tailed *post-hoc* test. The accepted level of significance was $p \leq 0.05$.

3. Results

3.1. Histological identification and quantification of the cholinergic and dopaminergic neuronal loss

The quantification of cholinergic and/or dopaminergic neuronal loss along with the corresponding individual examples of histological identification are depicted in **Fig. 2**.

In the PPT lesioned rats (with PD cholinopathy) the mean cholinergic neuronal loss for each brain side was > 22% throughout the overall rostro-caudal PPT dimension, with a maximum loss of 30.68 ± 6.28%, being the most caudally (**Fig. 2A**, PPT lesion).

In the SNpc lesioned rats (with hemiparkinsonism) the mean dopaminergic neuronal loss throughout the overall rostro-caudal SNpc dimension was > 56%, with a maximum loss of 92.64 ± 0.89%, also being the most caudally (**Fig. 2A**, SNpc lesion).

As depicted by the individual examples (**Fig. 2B-C**), the bilateral PPT (**Fig. 2B**, right panels) and unilateral SNpc (**Fig. 2C**) lesions were incomplete but selective, and always within the boundaries of the targeted nucleus.

In the SNpc/PPT lesioned rats (which had hemiparkinsonism with PD cholinopathy) the mean cholinergic neuronal loss for each brain side was > 27% throughout the overall rostro-caudal PPT dimension, with a maximum loss of 36.99 ± 2.85% at 7.50-8.00 mm caudally from

the bregma (**Fig. 2A**, bottom left panel, SNpc/PPT lesion), whereas the mean dopaminergic neuronal loss throughout the overall rostro-caudal SNpc dimension was > 48%, with a maximum loss of 72.93 ± 12.83% being the most caudally (**Fig. 2A,** bottom right panel, SNpc/PPT lesion).

Due to the possibility that the PPT cholinergic neuronal loss might have contributed to the additional death of the SNpc dopaminergic neurons and *vice versa*, we compared the mean number of NADPH – diaphorase positively stained cells in the PPT lesioned rats *versus* the SNpc/PPT lesioned rats, as well as the mean number of TH positively stained cell in the SNpc lesioned rats *versus* the SNpc/PPT lesioned rats for each stereotaxic range. We did not demonstrate any statistically significant difference in the dopaminergic neuronal loss between the SNpc lesioned and SNpc/PPT lesioned rats ($z \geq -0.91$; $p \geq 0.62$). However, we did show a higher cholinergic deficit in the SNpc/PPT lesioned vs. SNpc lesioned rats, but only for one stereotaxic range, at 7.50-8.00 mm caudally from the bregma ($z = -2.52$; $p = 0.01$).

3.2. Local alterations in the sleep architecture and Wake/NREM/REM episode dynamics in hemiparkinsonian rats

In contrast to PD cholinopathy (PPT lesion), which did not change the sleep/wake state architecture ($z \geq -0.84$; $p \geq 0.40$; **Table 1**), both groups of hemiparkinsonian rats (hemiparkinsonism – SNpc lesion and hemiparkinsonism complicated with PD cholinopathy – SNpc/PPT lesion) demonstrated a prolonged Wake duration in both the motor cortex and the hippocampus ($z \geq -3.26$; $p \leq 0.04$), with no change in NREM and REM duration ($z \geq -1.68$; $p \geq 0.09$; **Table 1**).

Further analysis of the Wake/NREM/REM episode dynamics enabled us to reveal severe motor cortical and hippocampal sleep fragmentation in both groups of hemiparkinsonian rats (SNpc lesion and SNpc/PPT lesion), showing that the prolonged Wake duration resulted only from an increased number of Wake episodes ($z \geq -2.74$; $p \leq 0.04$; **Table 1**).

Conversely, an increased number of the hippocampal NREM episodes in both groups of the hemiparkinsonian rats (SNpc lesion and SNpc/PPT lesion) ($z \geq -2.93$; $p \leq 0.01$) did not affect the NREM sleep duration due to the shortened NREM episodes ($z \geq -2.93$; $p \leq 0.01$; **Table 1**). However, hippocampal REM sleep disorder, caused particularly by the increased number of shortened REM episodes ($z \geq -2.93$; $p \leq 0.01$; **Table 1**), was shown only in the hemiparkinsonian rats with PD cholinopathy.

The group distributions of the mean number of Wake/NREM/REM episodes over their duration (in minutes) are depicted in **Fig. 3**. The group distribution of Wake episodes showed an increased number of Wake episodes of all durations in the motor cortex (**Fig. 3A**) and the

hippocampus (**Fig. 3B**), in both groups of hemiparkinsonian rats (SNpc lesion and SNpc/PPT lesion), that ultimately did not affect the mean duration of Wake episodes (**Table 1**).

In contrast, the group distribution of the hippocampal NREM and REM episodes showed an increased number of shorter and a decreased number of longer NREM and REM episodes (**Fig. 3B,** middle and bottom panel), resulting in a decreased mean duration of NREM episodes in both groups of hemiparkinsonian rats (**Table 1**, SNpc and SNpc/PPT lesions). However, the alteration in the hippocampal REM episodes dynamic (**Fig. 3B**, bottom panel) resulted in an overall decreased mean duration of REM episodes (**Table 1**) only in the hemiparkinsonian rats with PD cholinopathy (SNpc/PPT lesion).

3.3. Local NREM/REM EEG microstructure in hemiparkinsonian rats

In this study, we particularly analyzed the EEG microstructure of common (simultaneous) motor cortical and hippocampal NREM and REM sleep (**Fig. 4**). In contrast to PD cholinopathy, which only altered hippocampal NREM sleep by increasing the delta amplitude and decreasing the beta amplitude (**Fig. 4B**; $z \geq -3.26$; $p \leq 0.02$), the hemiparkinsonian rats exhibited more severe NREM/REM sleep disturbances.

Specifically, the most consistent alteration in the EEG microstructure at the onset of the dopaminergic deficit in both groups of hemiparkinsonian rats was an augmented NREM/REM theta amplitude in the motor cortex (**Fig. 4A**) and the hippocampus (**Fig. 4B**) ($z \geq -5.02$; $p \leq 0.04$). This theta amplitude augmentation was followed by attenuated delta and augmented sigma amplitudes during NREM within the motor cortex in both groups of hemiparkinsonian rats (**Fig. 4A**, NREM panels; $z \geq -3.39$; $p \leq 0.02$). On the other hand, the augmented theta amplitude during REM in the hippocampus of hemiparkinsonian rats (that is the SNpc lesioned rats) was followed by attenuated sigma and beta amplitudes (**Fig. 4B**, REM panels; $z \geq -2.72$; $p \leq 0.01$).

In addition, we demonstrated inverse NREM/REM beta amplitude alterations within the motor cortex (augmented vs. attenuated beta amplitude) in the hemiparkinsonian rats with PD cholinopathy (**Fig. 4A**, bottom panels; $z \geq -2.23$; $p \leq 0.03$) in contrast to the hippocampal attenuated sigma and beta amplitudes found only during REM in the hemiparkinsonian rats (**Fig. 4B**, REM panels). This indicated the topographically and NREM/REM state-related distinct impact of the impaired SNpc dopaminergic control on the beta and sigma oscillation amplitudes.

However, in both groups of hemiparkinsonian rats, the impaired SNpc dopaminergic control during the motor cortical and hippocampal REM was expressed as an attenuated beta amplitude (**Fig. 4A, B**, REM panels; $z \geq -2.72$; $p \leq 0.03$).

Moreover, our results demonstrated the opposite impact of the impaired dopaminergic *versus* cholinergic control on the delta and beta oscillation amplitudes during NREM in the hippocampus as well as in the motor cortex *versus* the hippocampus (**Fig. 4A**, NREM panels vs. **Fig. 4B**, NREM panels).

3.4. Spontaneous locomotor activity and habitual response in hemiparkinsonian rats

There was no alteration in spontaneous basal locomotor activity in any of experimental groups ($\chi^2 = 1.34$; p=0.86; **Fig. 5A**). In addition, we did not observe any alteration in either the stereotypic or the vertical activity ($\chi^2 \geq 1.89$; $p \geq 0.49$; data not shown).

The spatial habituation test (**Fig. 5B**) showed a decline in locomotor activity across sessions in both control groups (the physiological controls and the implanted controls; $\chi^2 \geq 6.25$; $p \leq 0.04$; $z \geq -2.88$; $p \leq 0.05$) indicating a physiological habitual response. This physiological habitual response was also demonstrated in the PPT lesioned rats ($\chi^2 = 9.09$; $p = 0.01$; $z \geq -2.72$; $p \leq 0.01$). However, both groups of hemiparkinsonian rats showed a lack of a physiological habitual response, indicating impaired spatial memory abilities ($\chi^2 \geq 0.98$; $p \geq 0.11$).

4. Discussion

We demonstrated severe prodromal sleep disturbances in hemiparkinsonian rats, mainly expressed as sleep fragmentation and distinct local NREM/REM EEG microstructure alterations.

The dopaminergic deficit induced by the SNpc lesion prolonged the motor cortical and hippocampal Wake duration in both groups of hemiparkinsonian rats, with no change in NREM and REM sleep duration (**Table 1**). This Wake prolongation was caused by an increased number of Wake episodes of all durations, with no change in their mean duration (**Table 1, Fig. 3**). This Wake prolongation shown at the onset of impaired dopaminergic control is in accordance with an earlier study that showed long-lasting sleep fragmentation from 14 to 42 days following the unilateral lesion of the SNpc (Ciric et al., 2019).

In this study, although stable in duration, the hippocampal NREM sleep was also fragmented in both groups of hemiparkinsonian rats, comprising an increased number of shorter NREM episodes (**Table 1, Fig. 3B**). However, only hemiparkinsonism complicated with PD cholinopathy induced hippocampal REM sleep fragmentation, due to an increased number of shorter REM sleep episodes (**Table 1, Fig. 3B**).

Furthermore, we demonstrated that the main EEG microstructure alteration in both groups of hemiparkinsonian rats was augmented theta amplitude during NREM and REM sleep (**Fig. 4**), indicating the general and sleep-state unrelated impact of the impaired dopaminergic

control at the level of the motor cortex and the hippocampus. In addition, this augmented theta amplitude was followed by an augmented sigma and attenuated delta amplitude only during NREM sleep in the motor cortex in both groups of hemiparkinsonian rats (**Fig. 4A**).

By contrast to these common alterations in the EEG microstructure in the motor cortex and the hippocampus in both groups of hemiaparkinsonian rats, during hippocampal REM sleep, the augmented theta amplitude was followed by attenuated sigma and beta amplitudes only in the hemiparkinsonian rats (**Fig. 4B**). Moreover, there was an inversion of the beta amplitude alteration during NREM and REM sleep in the motor cortex (augmented vs. attenuated beta amplitude) in the hemiparkinsonian rats with PD cholinopathy (**Fig. 4A**, bottom panels).

All these results suggest, beside the dopaminergic general and state-unrelated role in theta oscillations control (Ciric et al., 2019), the important, topographically, and NREM/REM related distinct role of the dopaminergic control of EEG delta, sigma and beta oscillations, and particular the importance of the REM neurochemical regulatory substrate in the dopaminergic control of beta oscillations.

Although impaired dopaminergic control during REM sleep has commonly been expressed as an attenuated beta amplitude in the motor cortex and the hippocampus, in this study we have shown the opposite impact of the impaired dopaminergic versus cholinergic control on the delta and beta oscillation amplitudes during NREM in the hippocampus, as well as in the motor cortex *versus* the hippocampus (**Fig. 4A**, NREM panels vs. **Fig. 4B**, NREM panels).

Sleep disorders are among the most frequent non-motor symptoms of PD (Schapira et al., 2017; Medeiros et al., 2019). With sleep regulating structures being affected prior to the SNpc degeneration (Braak et al., 2004), sleep disturbances such as insomnia, sleep fragmentation, RBD, restless leg syndrome, and excessive daytime sleepiness usually appear in the prodromal stage, preceding the motor symptoms by years or even decades (Schapira et al., 2017). It has been demonstrated that the dopaminergic nigrostriatal pathway is closely involved in the regulation of sleep patterns, particularly of REM sleep (Lima et al., 2007), along with the PPT cholinergic system (Datta and MacLean, 2007; Chambers et al., 2020). Moreover, based on the physiological association in sleep regulation between the PPT and the basal ganglia (BG), a new circuitry for sleep regulation has been proposed, being a triad comprising the PPT, the SNpc and the striatum (Targa et al., 2016). Thus, both the cholinergic and dopaminergic system are implicated in sleep control and could be severely compromised in PD pathology (Lima et al., 2007; Mena-Segovia et al., 2004; Perez-Lloret and Barrantes, 2016).

The dopaminergic and cholinergic systems operate in a dynamic balance that relies on reciprocal connections between the PPT and the BG, and this relationship is crucial for the normal functioning of both the BG and the PPT (Mena-Segovia et al., 2004; Lester et al., 2010). This interconnectivity is achieved at several levels and includes the BG output nuclei (the substantia nigra pars reticulata – SNpr and the internal globus pallidus – GPi), as well as the subthalamic nucleus (STN) and the SNpc (Mena-Segovia et al., 2008). In addition, one recent study demonstrated that the PPT, along with the laterodorsal tegmental nucleus, constitute the only external source of acetylcholine to the striatum (Dautan et al., 2016). This puts the PPT cholinergic neurons in a position to modulate the activity of the striatal system, as well as the activity of the BG. Due to predominantly excitatory projections, the activation of the PPT cholinergic neurons facilitates the BG output, induces a burst firing of DA neurons, and an increase in the striatal DA release, resulting in locomotor activity (Mena-Segovia et al., 2008). On the other hand, PPT activity is modulated by inhibitory inputs from the BG output nuclei and excitatory inputs from the STN (Mena-Segovia et al., 2004, 2008). Since PD neuropathology certainly disturbs this balance, and due to the reciprocal connections between the PPT cholinergic and the nigrostriatal dopaminergic neurons, the simultaneous decrease in both cholinergic and dopaminergic tone may potentially lead to severe neurodegeneration (Chambers et al., 2020). However, in our present study the simultaneous lesions of the PPT and the SNpc did not aggravate the overall cholinergic or dopaminergic neuronal loss in the SNpc/PPT lesioned rats at the onset of hemiparkinsonian neuropathology (**Fig. 2A**).

In contrast to another recent study, where rats with PD cholinopathy showed a decline in locomotor activity up to 91 days following the bilateral PPT lesion (Ciric et al., 2018), in this study, the behavioral assessments at the onset of each PD neuropathology did not reveal any locomotor deficit. However, we did find, beside the local sleep disorders, alterations of habitual response in both groups of hemiparkinsonian rats (**Fig. 5**), which indicated impaired spatial memory abilities at the onset of the dopaminergic control impairment.

Our study has demonstrated severe prodromal local sleep disturbances in hemiparkinsonian rats expressed as sleep fragmentation and distinct local NREM/REM EEG microstructure alterations. Alongside the state-unrelated role of the dopaminergic control of theta oscillations and NREM/REM related sigma and beta oscillations, we have shown that the underlying REM neurochemical regulatory substrate is particularly important in the dopaminergic control of beta oscillations. Regarding the local diversity of sleep disorders, this study presents the opposite impact of the dopaminergic *versus* cholinergic control on the delta

and beta oscillation amplitudes in the hippocampus, as well as in the motor cortex, *versus* the hippocampus during NREM sleep.

All these distinct prodromal local sleep disorders and the dopaminergic vs. cholinergic impacts on the NREM/REM EEG microstructure alterations are of fundamental importance for the further development and follow-up of PD-modifying therapies, and for the identification of patients who are at risk of developing PD.

Acknowledgement: This work was supported by a Serbian Ministry of Education, Science and Technological Development Grant OI 173022.

Reference

1. Andrzejewski, K., Budzinska, K., Zaremba, M., Kaczynska, K., 2016. Hypoxic ventilatory response after dopamine D2 receptor blokade in unilateral rat model of Parkinson's disease. Neuroscience 316, 192-200. https://doi.org/10.1016/j.neuroscience.2015.12.019.
2. Błaszczyk, J.W., 2016. Parkinson's Disease and Neurodegeneration: GABA-Collapse Hypothesis. Front. Neurosci. 10, 269. https://doi.org/10.3389/fnins.2016.00269.
3. Blesa, J., Przedborski, S., 2014. Parkinson's disease: animal models and dopaminergic cell vulnerability. Front. Neuroanat. 8, 155. https://doi.org/10.3389/fnana.2014.00155.
4. Boeve, B.F., Silber, M.H., Saper, C.B., Ferman, T.J., Dickson, D.W., Parisi, J.E., Benarroch, E.E., Ahlskog, J.E., Smith, G.E., Caselli, R.C., Tippman-Peikert, M., Olson, E.J., Lin, S.C., Young, T., Wszolek, Z., Schenck, C.H., Mahowald, M.W., Castillo, P.R., Del Tredici, K., Braak, H., 2007. Pathophysiology of REM sleep behaviour disorder and relevance to neurodegenerative disease. Brain 130, 2770–2788. https://doi.org/10.1093/brain/awm056.
5. Bohnen, N.I., Albin, R.L., 2011. The cholinergic system and Parkinson disease. Behav. Brain Res. 221, 564–573. https://doi.org/10.1016/j.bbr.2009.12.048.
6. Bohnen, N.I., Müller, M.L., Kotagal, V., Koeppe, R.A., Kilbourn, M.R., Gilman, S., Albin, R.L., Frey, K.A., 2012. Heterogeneity of cholinergic denervation in Parkinson's disease without dementia. J. Cereb. Blood Flow Metab. 32, 1609–1617. https://doi.org/10.1038/jcbfm.2012.60.
7. Boucetta, S., Salimi, A., Dadar, M., Jones B.J., Collins, L.D., Dang-Vu, T.T., 2016. Structural Brain Alterations Associated with Rapid Eye Movement Sleep Behavior Disorder in Parkinson's Disease. Sci. Rep. 6, 26782. https://doi.org/10.1038/srep26782.
8. Braak, H., Ghebremedhin, E., Rüb, U., Bratzke, H., Del Tredici, K., 2004. Stages in the development of Parkinson's disease-related pathology. Cell Tissue Res. 318, 121–134. https://doi.org/10.1007/s00441-004-0956-9.
9. Chambers, N.E., Lanza, K., Bishop, C., 2020. Pedunculopontine nucleus degeneration contributes to both motor and non-motor symptoms of Parkinson's disease. Front. Pharmacol. 10, 1494. https://doi.org/10.3389/fphar.2019.01494.
10. Ciric, J., Kapor, S., Perovic, M., Saponjic, J., 2019. Alteration of sleep and sleep oscillations in the hemiparkinsonian rat. Front. Neurosci. 13, 148. https://doi.org/10.3389/fnins.2019.00148.
11. Ciric, J., Lazic, K., Kapor, S., Perovic, M., Petrovic, J., Pesic, V., Kanazir, S., Saponjic, J., 2018. Sleep disorder and altered locomotor activity as biomarkers of the Parkinson's disease cholinopathy in rat. Behav. Brain Res. 339, 79–92. https://doi.org/10.1016/j.bbr.2017.11.021.
12. Ciric, J., Lazic, K., Petrovic, J., Kalauzi, A., Saponjic, J., 2015. Aging induced cortical drive alterations during sleep in rats. Mech. Ageing Dev. 146–148, 12–22. https://doi.org/10.1016/j.mad.2015.03.002.
13. Ciric, J., Lazic, K., Petrovic, J., Kalauzi, A., Saponjic, J., 2016. Age-related disorders of sleep and motor control in the rat models of functionally distinct cholinergic neuropathology. Behav. Brain Res. 301, 273–286. https://doi.org/10.1016/j.bbr.2015.12.046.
14. Ciric, J., Lazic, K., Petrovic, J., Kalauzi, A., Saponjic, J., 2017. Sleep spindles as an early biomarker of REM sleep disorder in a rat model of Parkinson's disease cholinopathy. Transl. Brain Rhythm. 2, 1–11. https://doi.org/10.15761/TBR.1000111.

15. Datta, S., MacLean, R.R., 2007. Neurobiological mechanisms for the regulation of mammalian sleep–wake behavior: Reinterpretation of historical evidence and inclusion of contemporary cellular and molecular evidence. Neurosci. Biobehav. Rev. 31, 775–824. https://doi.org/10.1016/j.neubiorev.2007.02.004.
16. Dautan, D., Hacioğlu Bay, H., Bolam, J.P., Gerdjikov, T.V., Mena-Segovia, J., 2016. Extrinsic sources of cholinergic innervation of the striatal complex: A whole-brain mapping analysis. Front. Neuroanat. 10, 1. https://doi.org/10.3389/fnana.2016.00001.
17. GBD 2016 Parkinson's Disease Collaborators, 2018. Global, regional, and national burden of Parkinson's disease, 1990–2016: a systematic analysis for the Global Burden of Disease Study 2016. Lancet Neurol. 17, 939–953. https://doi.org/10.1016/S1474-4422(18)30295-3.
18. Gilmour, T.P., Piallat, B., Lieu, C.A., Venkiteswaran, K., Ramachandra, R., Rao, A.N., Petticoffer, A.C., Berk, M.A., Subramanian, T., 2011. The effect of striatal dopaminergic grafts on the neuronal activity in the substantia nigra pars reticulata and subthalamic nucleus in hemiparkinsonian rats. Brain 134, 3276-3289. https://doi.org/10.1093/brain/awr226.
19. Inglis, W.L., Semba, K., 1997. Discriminable excitotoxic effects of ibotenic acid, AMPA, NMDA and quinolinic acid in the rat laterodorsal tegmental nucleus. Brain Res. 755, 17–27. https://doi.org/10.1016/s0006-8993(97)00101-7.
20. Iranzo, A., Molinuevo, J.L., Santamaría, J., Serradell, M., Martí, M.J., Valldeoriola, F., Tolosa, E., 2006. Rapid-eye-movement sleep behaviour disorder as an early marker for a neurodegenerative disorder: a descriptive study. Lancet Neurol. 5, 572–577. https://doi.org/10.1016/S1474-4422(06)70476-8.
21. Lazic, K., Petrovic, J., Ciric J., Kalauzi, A., Saponjic J., 2015. Impact of anesthetic regimen on the respiratory pattern, EEG microstructure and sleep in the rat model of cholinergic Parkinson's disease neuropathology. Neuroscience 304, 1-13. https://doi.org/10.1016/j.neuroscience.2015.07.020.
22. Lazic, K., Petrovic, J., Ciric, J., Kalauzi, A., Saponjic, J., 2017. REM sleep disorder following general anesthesia in rats. Physiol. Behav. 168, 41-54. https://doi.org/10.1016/j.physbeh.2016.10.013.
23. Lester, D.B., Rogers, T.D., Blaha, C.D., 2010. Acetylcholine–Dopamine interactions in the pathophysiology and treatment of CNS Disorders. CNS Neurosci. Ther. 16, 137-162. https://doi.org/10.1111/j.1755-5949.2010.00142.x.
24. Lima, M.M.S., Andersen, M.L., Reksidler, A.B., Vital, M.A.B.F., Tufik, S., 2007. The role of the substantia nigra pars compacta in regulating sleep patterns in rats. PLoS ONE 2(6), e513. https://doi.org/10.1371/journal.pone.0000513.
25. Mayeux, R., Stern, Y., 2012. Epidemiology of Alzheimer Disease. Cold Spring Harb. Perspect. Med. 2, a006239. https://doi.org/10.1101/cshperspect.a006239.
26. Medeiros, D.C., Lopes Aguiar, C., Moraes, M.F.D., Fisone, G., 2019. Sleep disorders in rodent models of Parkinson's Disease. Front. Pharmacol. 10, 1414. https://doi.org/10.3389/fphar.2019.01414.
27. Mena-Segovia, J., Bolam, J.P., Magill, P.J., 2004. Pedunculopontine nucleus and basal ganglia: distant relatives or part of the same family. Trends. Neurosci. 27, 585-588. https://doi.org/10.1016/j.tins.2004.07.009.
28. Mena-Segovia, J., Winn, P., Bolam, J.P., 2008. Cholinergic modulation of midbrain dopaminergic systems. Brain Res. Rev. 58, 265-271. https://doi.org/10.1016/j.brainresrev.2008.02.003.
29. Müller, M.L., Albin, R.L., Kotagal, V., Koeppe, R.A., Scott, P.J., Frey, K.A., Bohnen, N.I., 2013. Thalamic cholinergic innervation and postural sensory integration function in Parkinson's disease. Brain 136, 3282–3289. https://doi.org/10.1093/brain/awt247.

30. Oliveira, L.M., Tuppy, M., Moreira, T.S., Takakura, A.C., 2017. Role of the locus coeruleus catecholaminergic neurons in the chemosensory control of breathing in a Parkinson's disease model. Exp. Neurol. 293, 172-180. https://doi.org/10.1016/j.expneurol.2017.04.006.
31. Paxinos, G., Watson, C., 2005. The rat brain in stereotaxic coordinates, fifth ed. Academic Press, San Diego. (ISBN: 9780080474120).
32. Paxinos, G., Watson, C., Carrive, P., Kirkcaldie, M., Ashwell, K.W.S., 2009. Chemoarchitectonic Atlas of the rat brain, second ed. Academic Press, London. (ISBN: 978-0123742377).
33. Perez-Lloret, S., Barrantes, F.J., 2016. Deficits in cholinergic neurotransmission and their clinical correlates in Parkinson's disease. npj Parkinsons Dis. 2, 16001. https://doi.org/10.1038/npjparkd.2016.1.
34. Petrovic, J., Ciric, J., Lazic, K., Kalauzi, A., Saponjic, J., 2013a. Lesion of the pedunculopontine tegmental nucleus in rat augments cortical activation and disturbs sleep/wake state transitions structure. Exp. Neurol. 247, 562–571. https://doi.org/10.1016/j.expneurol.2013.02.007.
35. Petrovic, J., Lazic, K., Ciric, J., Kalauzi, A., Saponjic, J., 2013b. Topography of the sleep/wake states related EEG microstructure and transitions structure differentiates the functionally distinct cholinergic innervation disorders in rat. Behav. Brain Res. 256, 108–118. https://doi.org/10.1016/j.bbr.2013.07.047.
36. Petrovic, J., Lazic, K., Kalauzi, A., Saponjic, J., 2014. REM sleep diversity following the pedunculopontine tegmental nucleus lesion in rat. Behav. Brain Res. 271, 258–268. https://doi.org/10.1016/j.bbr.2014.06.026.
37. Pienaar, I.S., van de Berg, W., 2013. A non-cholinergic neuronal loss in the pedunculopontine nucleus of toxin-evoked Parkinsonian rats. Exp. Neurol. 248, 213–223. https://doi.org/10.1016/j.expneurol.2013.06.008.
38. Rajkovic, N., Ciric, J., Milosevic, N., Saponjic, J., 2019. Novel application of the gray-level co-occurrence matrix analysis in the parvalbumin stained hippocampal gyrus dentatus in distinct rat models of Parkinson's disease. Comput. Biol. Med. 115, 103482. https://doi.org/10.1016/j.compbiomed.2019.103482.
39. Rodriguez, J.J., Montaron, M.F., Aurousseau, C., Le Moal, M., Abrous, D.N., 1999. Effects of amphetamine and cocaine treatment on c-Fos, Jun-B, and Krox-24 expression in rats with intrastriatal dopaminergic grafts. Exp. Neurol. 159, 139–152. https://doi.org/10.1006/exnr.1999.7129.
40. Saponjic, J., Petrovic, J., Ciric, J., Lazic, K., 2016. Disorders of sleep and motor control during the impaired cholinergic innervation in rat – relevance to Parkinson's disease. In: Dorszewska, J. and Kozubski, W. (Eds.), Challenges in Parkinson's Disease. InTech Rijeka, Rijeka, Croatia, pp: 135-153. https://doi.org/10.5772/62949.
41. Schapira, A.H.V., Chaudhuri, K.R., Jenner P., 2017. Non-motor features of Parkinson disease. Nat. Rev. Neurosci. 18(7), 435-450. https://doi.org/10.1038/nrn.2017.62.
42. Targa, A.D.S., Rodrigues, L.S., Noseda, A.C.D., Aurich, M.F., Andersen, M.L., Tufik, S., da Cunha, C., Lima, M.M.S., 2016. Unraveling a new circuitry for sleep regulation in Parkinson's disease. Neuropharmacology. 108, 161-171. https://doi.org/10.1016/j.neuropharm.2016.04.018.
43. Videnovic, A., Golombek, D., 2013. Circadian and sleep disorders in Parkinson's disease. Exp. Neurol. 243, 45–56. https://doi.org/10.1016/j.expneurol.2012.08.018.

Figure captions

Table 1. Local Wake/NREM/REM episode dynamics in hemiparkinsonian rats. The mean duration of the Wake/NREM/REM sleep/6 hours ± SE (minutes) with the mean number and mean duration/6 hours ± SE (minutes) of the Wake/NREM/REM episodes within the motor cortex (MCx) and the hippocampus (Hipp).

Fig. 1. The experimental time-line. Control-p – the physiological control; Control-i – the implanted control; PPT lesion – PD cholinopathy; SNpc lesion – hemiparkinsonism; SNpc/PPT lesion – hemiparkinsonism with PD cholinopathy.

Fig. 2. Histological identification and quantification of the cholinergic and dopaminergic neuronal loss. Quantification of the cholinergic (Ach) and/or dopaminergic (DA) neuronal loss in PD cholinopathy (PPT lesion), hemiparkinsonism (SNpc lesion) and hemiparkinsonism with PD cholinopathy (SNpc/PPT lesion), counted in three stereotaxic ranges, defined on the basis of the overall PPT or SNpc rostro-caudal dimension (**A**). An individual example of the histological identification of the PPT lesion by NADPH – diaphorase staining (**B**) (right panels) vs. control brain (left panels), in three brain sections, representing each stereotaxic range of the overall rostro-caudal dimension of the PPT. In this SNpc/PPT lesioned rat, the cholinerginc neuronal loss was 26.25% on one side and 34.22% on the other side at 7.47 mm caudally for bregma, 23.81% on one side and 42.86% on the other side at 7.97 mm caudally from bregma, and 29.36% on one side and 54.40% on the other side at 8.29 mm caudally from bregma. Individual examples of the histological identification of the SNpc lesion by tyrosine hydroxylase (TH) imunohistochemistry (**C**) in three brain sections, representing each stereotaxic range of the overall rostro-caudal dimension of the SNpc. In this SNpc/PPT lesioned rat the dopaminergic neuronal loss was 2.33% at 5.04 mm caudally from bregma, 47.92% at 5.36 mm caudally from bregma, and 91.31% at 6.03 mm caudally from bregma. PPT – pedunculopontine tegmental nucleus pars compacta; xcsp – decussation of the superior cerebellar peduncle; MnR – median raphe nucleus; LDT – laterodorsal tegmental nucleus; asterisks indicate the lesioned PPT. Scale bar 200 μm. SNpc – substantia nigra pars compacta; VTA – ventral tegmental area; asterisks indicate the lesioned SNpc. Scale bar 400 μm.

Fig. 3. Local NREM/REM episode dynamics in hemiparkinsonian rats. The group distributions of the Wake/NREM/REM mean number of episodes/6 hours over their durations (minutes) within the motor cortex (**A**) and the hippocampus (**B**). In these log-log distributions

each “horizontal stair” is placed above its corresponding duration, depicted on the x-axis in minutes – e.g. the group mean number/6 hours of 10 second episodes is placed above 10/60=0.17 minutes and so on. The first three episode durations are indicated below the “stair line” of the two upper panels as 10, 20 and 30, presenting the group mean number/6 hours of Wake 10, 20, and 30 second episodes. The missing lines in the distributions depict the zero group mean number of episodes that causes the logarithms to be defined as “not a number”.

Fig. 4. Local NREM/REM EEG microstructure in hemiparkinsonian rats. The group probability density distributions/ 6 hours of the motor cortical (**A**) and the hippocampal (**B**) delta, theta, sigma, and beta amplitudes during NREM and REM sleep. Arrows indicate the statistically significant increase (arrows up) or decrease (arrows down) of the amplitude of a certain EEG frequency range in the corresponding experimental group at $p \leq 0.05$.

Fig. 5. Spontaneous locomotor activity and spatial habituation in hemiparkinsonian rats. Time dependent profiles for 5 minute periods during the session (left panel) and total distance travelled for the overall 30 minute session (right panel) for locomotor activity (**A**) and spatial habituation test (**B**). All comparisons were made with respect to the physiological controls (Control-p) and the implanted controls (Control-i). Asterisks indicate the statistically significant mean values at $p \leq 0.05$.

Table 1. Local Wake/NREM/REM episode dynamics in the hemiparkinsonian rats.

	Mean duration/6 h ± SE (min)			**Mean number of episodes/6 h ± SE**			**Mean duration of episodes/6 h ± SE (min)**		
	Wake	NREM	REM	Wake	NREM	REM	Wake	NREM	REM
MCx									
Control	61.17 ± 6.87	198.17 ± 13.36	100.33 ± 9.22	117.14 ± 9.68	310.57 ± 31.04	259.43 ± 33.09	0.48 ± 0.03	0.73 ± 0.12	0.40 ± 0.04
PPT lesion	65.38 ± 9.36	188.90 ± 11.20	105.40 ± 12.44	120.63 ± 18.61	319.13 ± 24.27	283.75 ± 36.86	0.55 ± 0.06	0.64 ± 0.09	0.38 ± 0.02
SNpc lesion	**93.17 ± 11.03**	187.73 ± 6.93	78.77 ± 13.12	**154.57 ± 12.35**	261.14 ± 23.84	183.57 ± 30.50	0.67 ± 0.07	0.77 ± 0.08	0.39 ± 0.03
SNpc/PPT lesion	**96.79 ± 9.66**	176.04 ± 15.45	86.83 ± 11.71	**180.50 ± 22.14**	296.33 ± 29.34	263.33 ± 20.98	0.58 ± 0.06	0.59 ± 0.10	0.36 ± 0.03
Hipp									
Control	53.17 ± 3.15	233.48 ± 12.53	73.02 ± 12.20	97.20 ± 4.99	146.00 ± 2.14	78.40 ± 5.02	0.52 ± 0.02	1.71 ± 0.03	0.77 ± 0.08
PPT lesion	60.21 ± 8.36	230.88 ± 14.48	68.58 ± 15.71	109.88 ± 11.83	181.00 ± 20.15	127.25 ± 29.49	054 ± 0.05	1.46 ± 0.25	0.57 ± 0.05
SNpc lesion	**87.81 ± 7.89**	210.71 ± 5.99	61.15 ± 10.24	**176.67 ± 27.13**	**222.17 ± 27.15**	88.83 ± 17.03	0.58 ± 0.06	**1.05 ± 0.13**	0.60 ± 0.09
SNpc/PPT lesion	**88.65 ± 9.84**	195.98 ± 13.52	75.04 ± 10.60	**194.25 ± 40.64**	**276.63 ± 40.02**	**215.50 ± 37.22**	0.52 ± 0.06	**0.84 ± 0.14**	**0.37 ± 0.02**

Bold numbers indicate statistically significant mean values at $p \leq 0.05$.

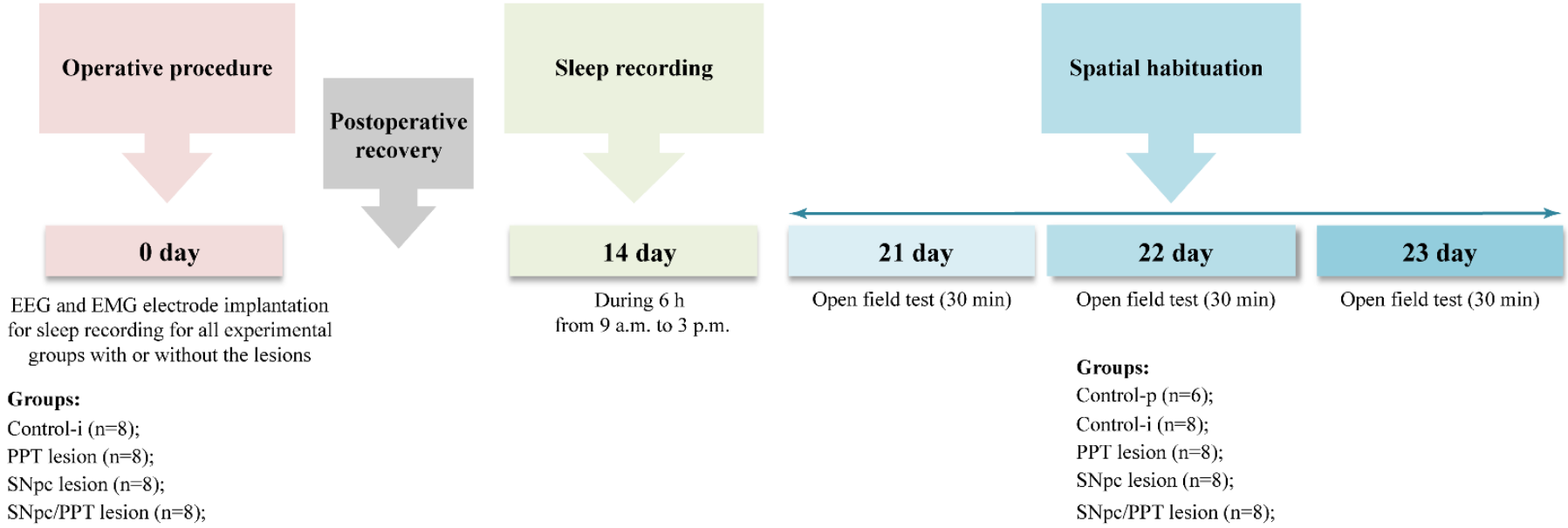
Operative procedure
Postoperative recovery
Sleep recording
Spatial habituation
0 day
14 day
21 day
22 day
23 day
EEG and EMG electrode implantation for sleep recording for all experimental groups with or without the lesions
Groups:
Control-i (n=8);
PPT lesion (n=8);
SNpc lesion (n=8);
SNpc/PPT lesion (n=8);
During 6 h from 9 a.m. to 3 p.m.
Open field test (30 min)
Open field test (30 min)
Open field test (30 min)
Groups:
Control-p (n=6);
Control-i (n=8);
PPT lesion (n=8);
SNpc lesion (n=8);
SNpc/PPT lesion (n=8);

Fig. 1.

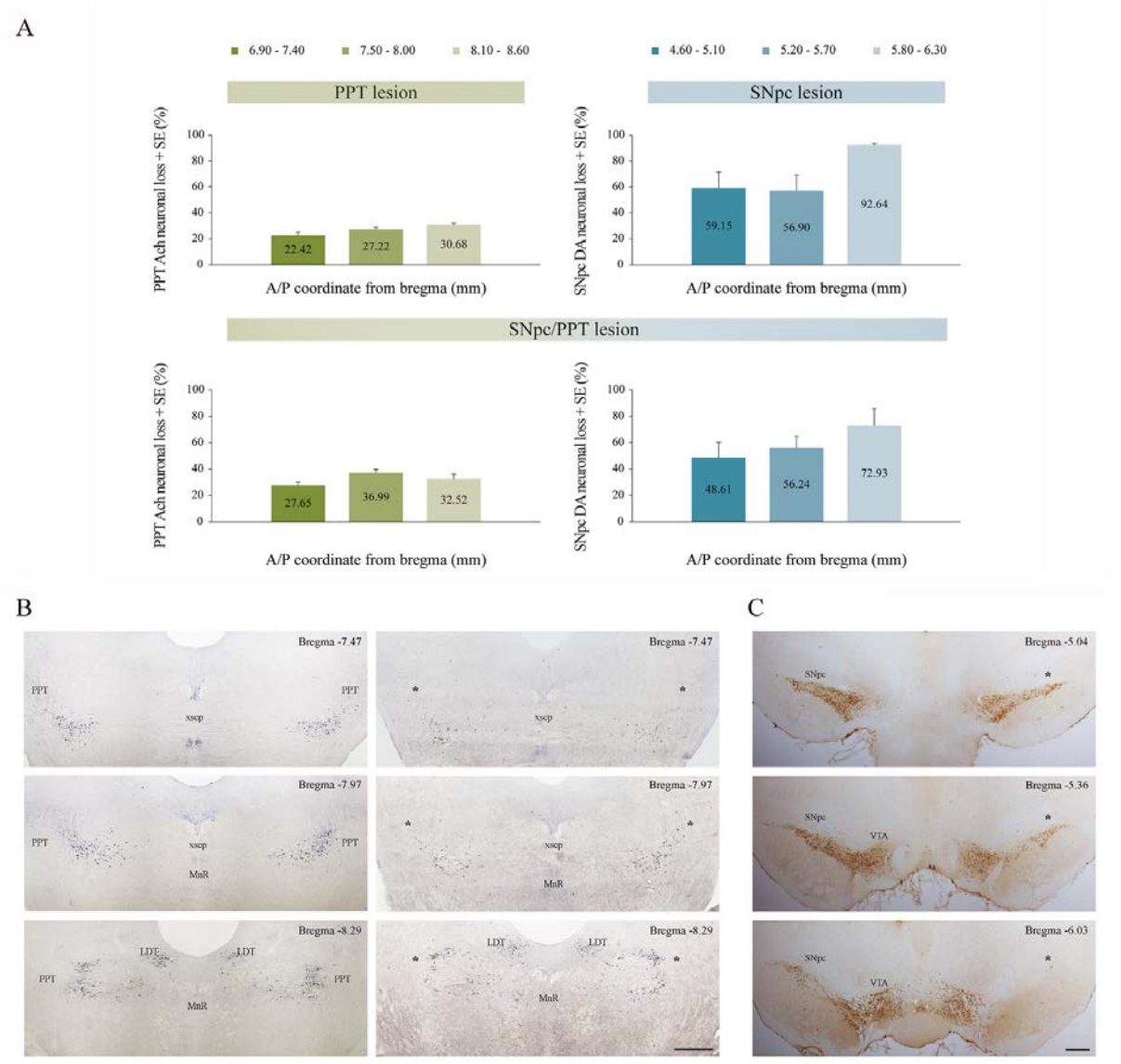
A
6.90 - 7.40
7.50 - 8.00
8.10 - 8.60
PPT lesion
PPT Ach neuronal loss + SE (%)
22.42
27.22
30.68
A/P coordinate from bregma (mm)
4.60 - 5.10
5.20 - 5.70
5.80 - 6.30
SNpc lesion
SNpc DA neuronal loss + SE (%)
59.15
56.90
92.64
A/P coordinate from bregma (mm)
SNpc/PPT lesion
PPT Ach neuronal loss + SE (%)
27.65
36.99
32.52
A/P coordinate from bregma (mm)
SNpc DA neuronal loss + SE (%)
48.61
56.24
72.93
A/P coordinate from bregma (mm)
B
C
Bregma -7.47
Bregma -7.97
Bregma -8.29
PPT
xscp
MnR
LDT
Bregma -5.04
Bregma -5.36
Bregma -6.03
SNpc
VTA

Fig. 2.

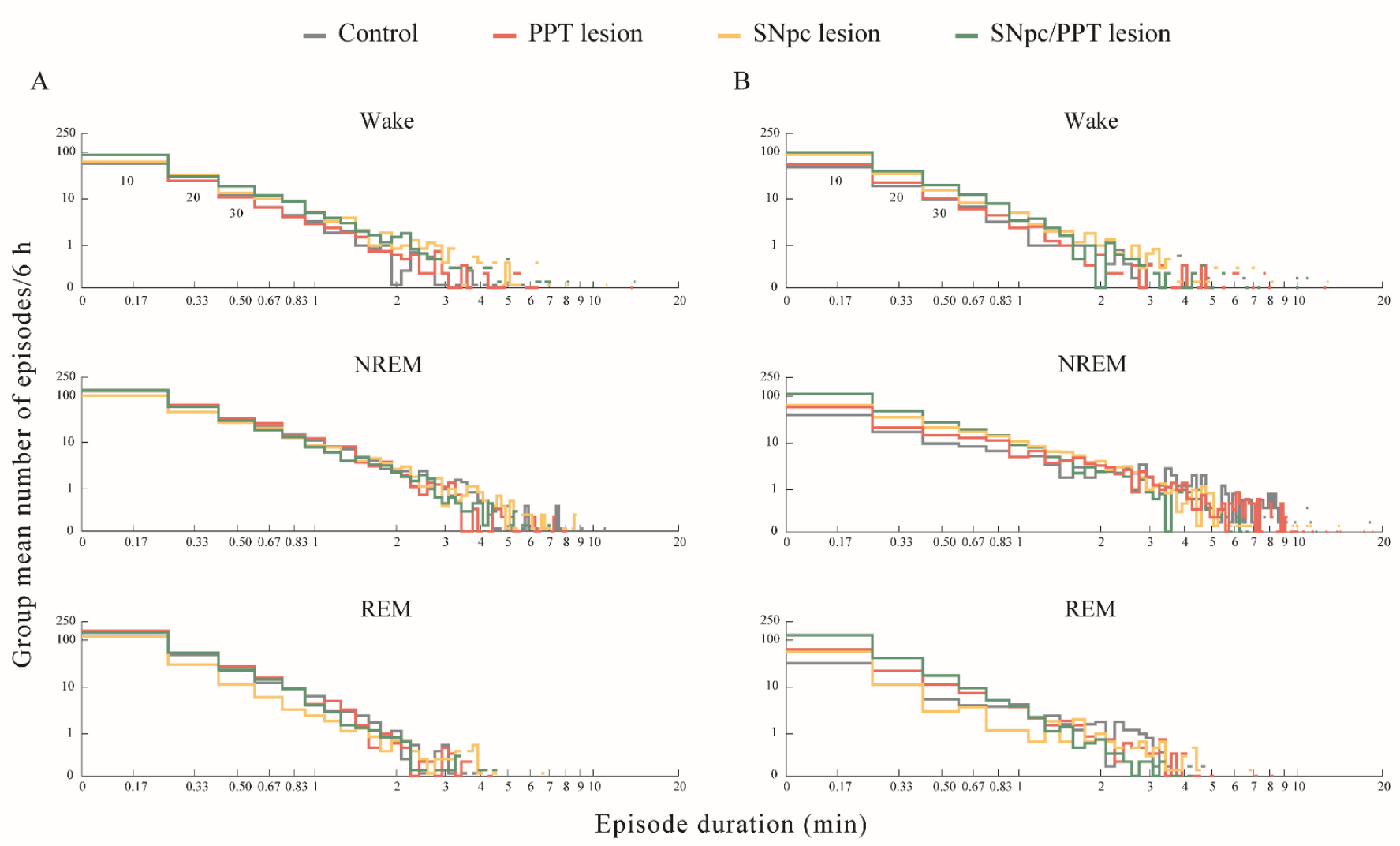
Control
PPT lesion
SNpc lesion
SNpc/PPT lesion
A
B
Wake
NREM
REM
Group mean number of episodes/6 h
Episode duration (min)

Fig. 3.

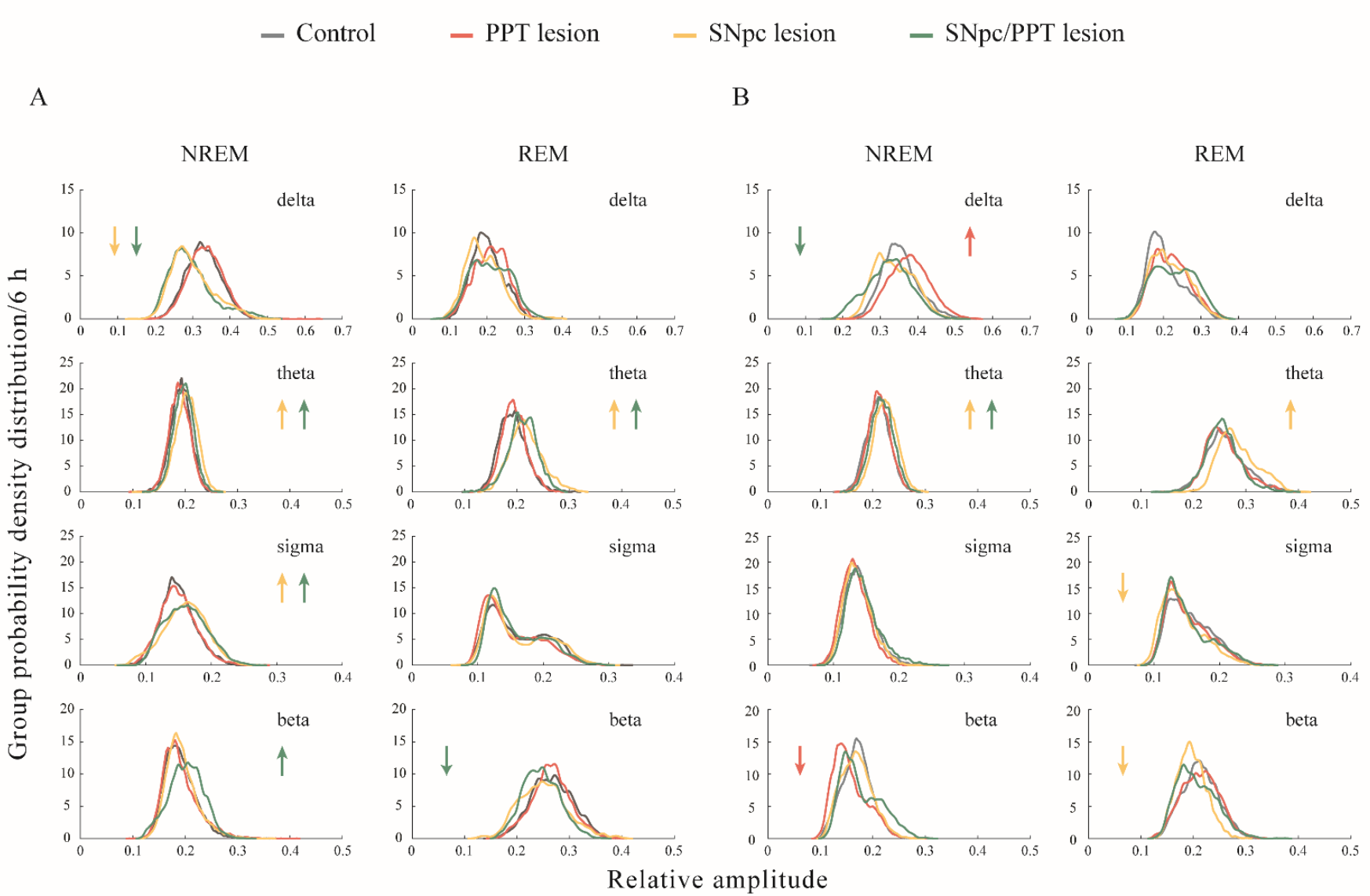
Control
PPT lesion
SNpc lesion
SNpc/PPT lesion
A
B
NREM
REM
NREM
REM
delta
theta
sigma
beta
Group probability density distribution/6 h
Relative amplitude

Fig. 4.

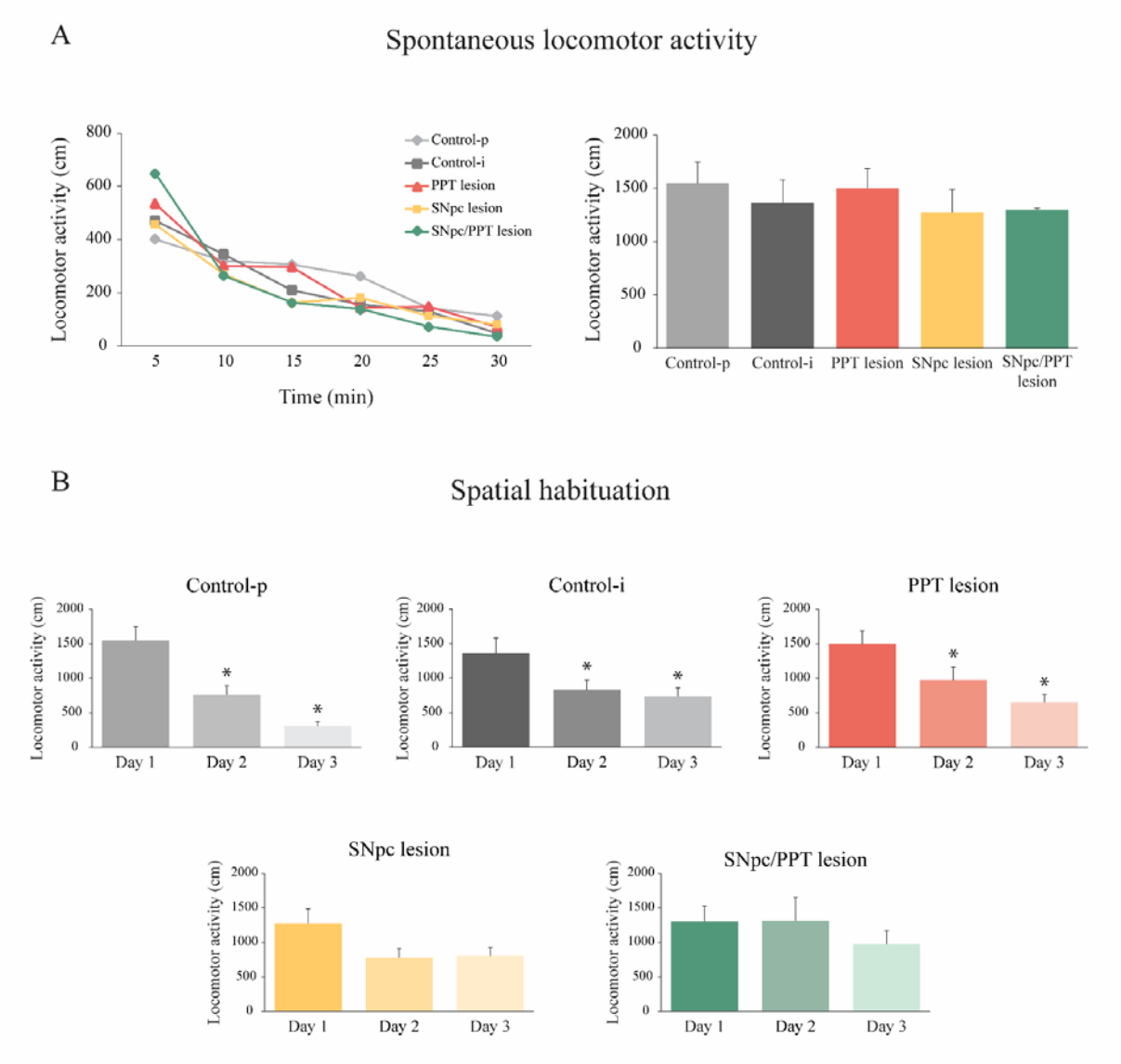
A
Spontaneous locomotor activity
Locomotor activity (cm)
Time (min)
Control-p
Control-i
PPT lesion
SNpc lesion
SNpc/PPT lesion
B
Spatial habituation
Day 1
Day 2
Day 3

Fig. 5.